White Dwarf Planetary Systems: insights regarding the fate of planetary systems

Amy Bonsor, Siyi Xu

Abstract Planetary material accreted by white dwarfs provides critical insights regarding the composition of planetary material. The analysis of polluted white dwarfs suggests that rocky planetary material similar in composition to bulk Earth is common, and that differentiation and collisions play a key role in planetary systems. Infrared observations track the accretion of dusty planetary material in discs that share many similarities with Saturn's rings, as well as proto-planetary discs. Planetary material arrives close to the star, scattered inwards from an outer planetary systems that has survived the star's evolution. White dwarf planetary systems provide key observational constraints that enable us to study the evolution of planetary systems under extreme conditions.

1 Introduction

Almost all stars where exo-planets have been detected to date will one day evolve to end their lives as white dwarfs. Theoretically even the fate of our own Solar System is uncertain [16]. Whilst we are unable to observe the evolution of our Solar System in real time, we can study nearby white dwarfs to try and infer what may happen to our Solar System and other planetary systems, once their host stars leave the main-sequence.

White dwarfs are the faint remnants of stars like our Sun. They have a typical mass of $0.6M_{\odot}$, but a radius of about Earth, and cool from a temperature of over one hundred thousand kelvin to a few thousand kelvin, in the age of the Universe. Stars

Amy Bonsor
Institute of Astronomy, University of Cambridge, Madingley Road, Cambridge, UK, CB3 0HA, e-mail: amy.bonsor@gmail.com

Siyi Xu
European Southern Observatory, Karl-Schwarzschild-Strasse 2, D-85748 Garching, Germany e-mail: sxu@eso.org

like our Sun, and up to a mass of about $8M_{\odot}$, swell to become giant stars. They loose a substantial fraction of their mass (between half and two thirds), mainly during the tip of the asymptotic giant branch, in a planetary nebulae. The compact remnant left behind becomes a white dwarf. Whilst the inner planetary system may be lost, swallowed in the giant star's expanding envelope, [49] show that rocky planets should survive exterior to $\sim$3 AU and gas giants initially exterior to $\sim$5 AU. Any surviving planetary system expands, due to adiabatic mass loss, and [73] show that the planetary system interior to 15AU should be devoid of giant planets, unless they have arrived in this region after the giant branch. Outer debris belts, outside of a few AU, will survive the star's evolution, albeit stripped of small planetesimals (up to tens of metre in size on the AGB), which are rapidly replenished by collisions during the early white dwarf phase [5].

Observationally it is very difficult to study white dwarf planetary systems directly. Detection of outer planets, or outer debris belts is difficult due to their low luminosity. The best way to study the planetary system orbiting a white dwarf is from observations of planetary material that has been accreted by *polluted* white dwarfs. A white dwarf should have an atmosphere that is pure hydrogen or helium. The presence of heavier elements indicates the recent accretion of material from exterior to the white dwarf. Over 30% of white dwarfs exhibit heavy elements in their spectra [87, 88, 41], the composition of which are consistent with rocky planetary material, in general similar to bulk Earth [36]. Alongside observations of gas and dust, polluted white dwarfs provide the best way to study the fate of planetary systems.

2 Planetary Systems Post-main Sequence

A white dwarf may be orbited by planets and (or) debris belts, exterior to a few au, that have survived the star's evolution. The most likely explanation for white dwarf pollution is that planetary material has been transported from this outer planetary system close enough to the star to be tidally disrupted (about a solar radius). Fragments from the disrupted planetary bodies accrete onto the star. There are few transport processes that lead to planetary material arriving this close to the white dwarf. For example, [5] show that Poynting-Robertson drag can only transport dust grains smaller than 20mm to the star, if they start exterior to 1au. Scattering remains the most effective mechanism at transporting planetary material from the outer planetary system down to the star. The accreted material could originate from a range of sources, asteroids, comets or planets. We use the term planetesimal to refer to any planetary body that is in a debris belt.

2.0.1 Dynamical instabilities following stellar mass loss

When a star loses mass, if the mass loss is adiabatic, the orbits of any planets or planetesimals spiral outwards. The planet's semi-major axis increases as

$$a_f = a_i \frac{M_f}{M_i}. \tag{1}$$

With a reduced central mass, the influence of any planetary bodies on one another increases. This can lead to dynamical instabilities. [12] illustrate how an initially stable configuration can become unstable following mass loss. Such instabilities can lead to planetary bodies scattered onto star-grazing orbits, which in turn can lead to the pollution of white dwarfs. White dwarf pollution could occur when planets (minor planets or exo-moons) themselves are scattered onto star-grazing orbits, or alternatively when planets scatter smaller bodies, either exo-moons, or planetesimals (asteroids or comets) onto star-grazing orbits. There is as yet no consensus in the literature regarding which process dominates, and probably all processes are occurring. However, important insights can be derived by considering the frequency, level and composition of the pollution. The scattering of larger bodies will be less frequent and lead to higher levels of pollution than the (continuous) scattering of smaller bodies, as shown by [79].

2.1 Planetesimals

The observational evidence for the presence of both planetesimals (debris belts) and planets in white dwarf systems is growing [78]. About 30% of A stars, the progenitors of most white dwarfs, exhibit an infrared excess from a debris belt [63]. When the star loses mass, the influence of any planets on the planetesimals in that system increases. This can lead to the scattering of planetesimals by planets. We can consider two scenarios.

In the first, the inner edge of a planetesimal belt is carved out by a planet that has cleared its chaotic zone of material. The width of the chaotic zone, for a planet on a circular orbit, is given by :

$$\frac{\delta a_{chaos}}{a_{pl}} = C \left(\frac{m_{pl}}{M_\odot} \right)^{2/7} \tag{2}$$

where C is a constant whose value is about 1.2, a_{pl} is the planet semi-major axis, m_{pl} is the planet mass and M_* is the stellar mass. As the stellar mass decreases, the size of the chaotic zone increases. This leads to increased scattering, as shown by [6] and [22] for eccentric planets. [6] show that a single planet at 30AU (or 60AU post-stellar mass loss), interior to a planetesimal belt, scatters sufficient material inwards in order to explain the observed white dwarf pollution, if there exists an interior planetary system that is similarly efficient at scattering planetesimals inwards as

our Solar System. [6] assume a distribution of planetesimal belt masses that fits the observations of debris discs around A stars [77], evolved to the start of the white dwarf phase [5]. The accretion rates from scattering fall off steeply with time after the start of the white dwarf phase.

In the second scenario, planetesimals are scattered due to the increase in width of unstable resonances. [14] show that the width of the interior mean-motion resonances with Jupiter in the asteroid belt increase following stellar mass loss. In the restricted three-body case, expanding for low eccentricities [48], the maximum libration width for interior first-order resonances is given by

$$\delta a_{max} = \pm \left(\frac{16 C_r e}{n} \right)^{1/2} \left(1 + \frac{C_r}{27 j_2^2 e^3 n} \right)^{1/2} - \frac{2 C_r a}{9 j_2 e n}, \tag{3}$$

where n is the mean motion of the planetesimal is proportional to the stellar mass, $n = \sqrt{\frac{GM_*}{a^3}}$, a, e are the semi-major axis and eccentricity of the planetesimal, C_r and j_2 are constants from the distributing function [48]. This width is inversely proportional to the stellar mass. As the star loses mass, many previously stable particles become unstable, as shown by Fig. 1. [14] use N-body simulations to determine the rate at which asteroids are scattered onto star-grazing orbits in the post-main sequence Solar System. They show that this mechanism can produce the observed accretion rates from polluted white dwarfs in a planetary system with an asteroid belt than has a mass ~ 820 times that of the Solar System's asteroid belt.

Fig. 1 shows that the difference in scattering rates between an exterior and interior planet is minimal, and the scattering rates are dominated by the planet and belt mass. Whilst more material survives in outer planetesimal belts, it is easier to transport material inwards from an inner planetesimal belt, and it is, therefore, currently not clear from the dynamics whether the accretion would be dominated by planetesimals that originate from planetesimal belts that are close to the star (exo-asteroid belts) or planetesimal belts that are further from the star (exo-Kuiper belts).

2.2 Planets

Dynamical instabilities and planet-planet scattering are thought to be a key feature of the early evolution of planetary systems e.g. [58]. Most instabilities occur early ($<$10Myr), after which planetary systems generally settle down to stable configurations [57]. Late-time instabilities are rare [57, 7]. Such stable configurations, however, may not remain stable following stellar mass loss on the giant branches. Analytically it can be shown that by reducing the stellar mass, the separation of two planets must increase in order for them to continue to be Hill stable [12, 70].

Planetary systems are chaotic and the exact dynamics depend on the exact configuration of individual systems. A wide range of numerical simulations have shown [12, 70, 50, 71] that instabilities can occur both during the giant branch evolution and in the white dwarf evolution that follows. Whilst the rate of instabilities de-

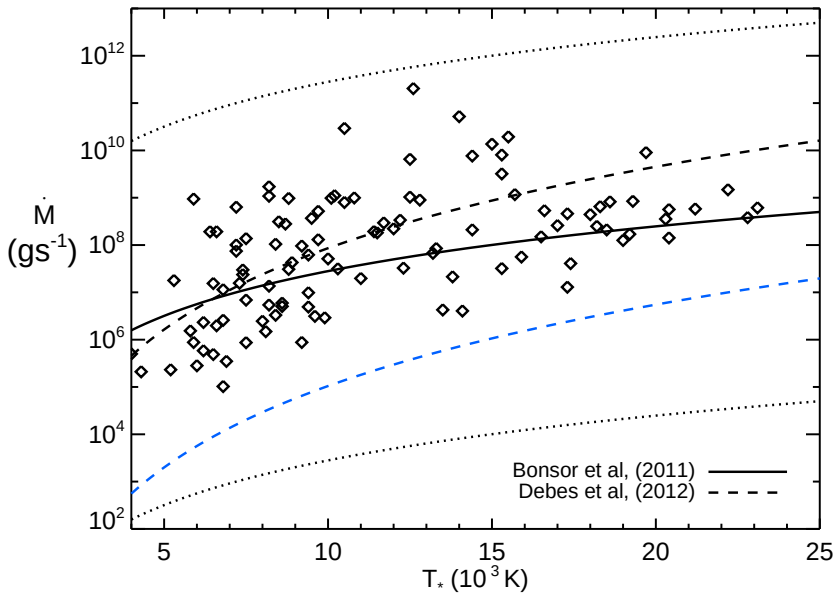

Fig. 1 The accretion rates derived from calcium for known white dwarfs, assuming a composition of bulk Earth (Farihi, personal communication). These are compared to the distribution of accretion rates fitted to the scattering simulations of [6], tracking scattering following the increase in width of the chaotic zone post-stellar mass loss (black solid line) , and [14], following the increase in width of internal resonances with a planet (black dashed line). The blue dashed line shows an asteroid with the mass of the current day asteroid belt, whereas the black dashed line shows a mass of 820 times the current day. The dotted lines show the minimum and maximum of the [6] distribution, depending on planet mass and belt mass.

creases significantly with time after the end of mass loss, instabilities can still occur long into the white dwarf phase [70]. Some instabilities lead to planets that approach close to the star, whilst others may scatter planets into regions where these planets then scatter planetesimals onto star-grazing orbits. The majority of planets are ejected following stellar mass loss [71], in addition to which non-adiabatic mass loss for objects on long period orbits can lead to the *escape* of planets or comets [68, 69].

2.3 Exo-moons

In our Solar System, many planets are orbited by several moons or satellites. [52] show that gravitational scattering amongst planets following stellar mass loss leads to the liberation of exo-moons. These exo-moons could, themselves be scattered

onto star-grazing orbits, or instead be scattered into a region where they readily scatter planetesimals onto star-grazing orbits, thus, leading to white dwarf pollution.

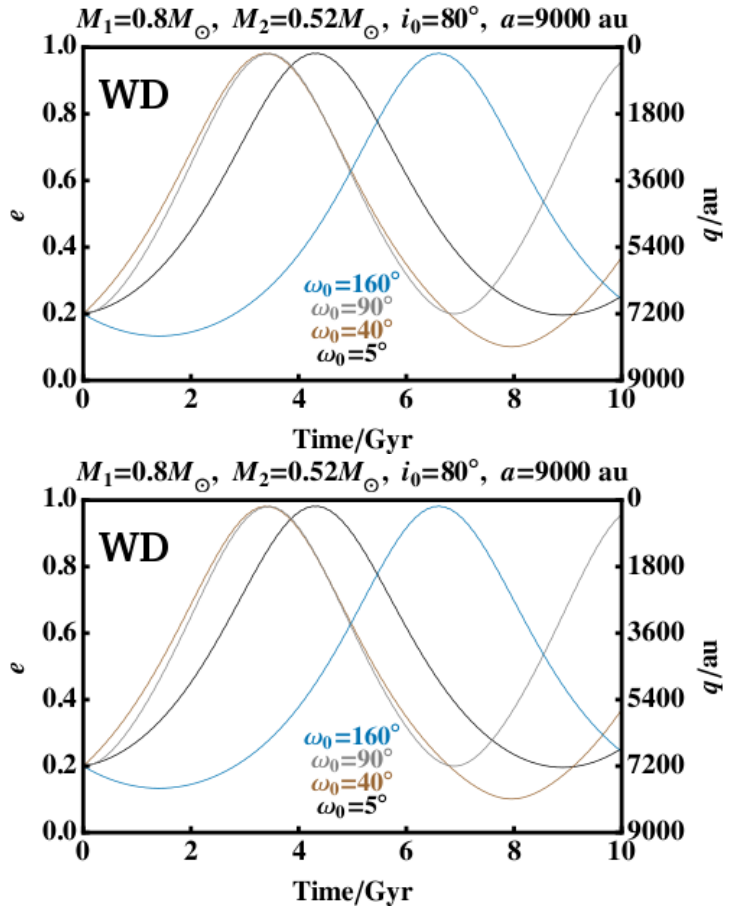

Fig. 2 A binary can have a first close approach (high eccentricity) during the white dwarf phase. Such a close approach could trigger instabilities that lead to white dwarf pollution. The figures show the evolution of an example binary's orbit due to Galactic tides; the top panel on the main-sequence and the bottom panel, during the white dwarf phase, following stellar mass loss. [8]

2.3.1 The influence of binary companions

The rate of dynamical instabilities induced by stellar mass loss necessarily decreases very steeply as a function of time after the end of stellar mass loss (or white dwarf cooling age). The presence of a binary companion can induce dynamical instabilities in a planetary system following stellar mass loss, even after Gyrs of stable evolution. This can lead to white dwarf pollution even in old white dwarfs, in a manner that is relatively independent of age.

It has been shown for main-sequence planetary systems, that whilst in general wide ($a > 1,000$AU) binary companions do not influence the dynamics of the planetary system, the orbit of the binary varies due to Galactic tides. During periods of 'close' pericentre passage, the binary may excite the eccentricities of planets, even ejecting them [38]. The increased eccentricity of exoplanets in systems with wide binary companions has been confirmed by observations [38]. The same scenario could be applied to white dwarf planetary systems. If the white dwarf is orbited by a wide binary companion, the planetary system may remain unperturbed for billions of years, before Galactic tides alter the orbit of the companion such that it induces dynamical instabilities in the planetary system. The increase in separation of the binary following stellar mass loss, increases the perturbations on the binary's orbit due to the Galactic tides, making it more likely for the first close approach of a binary to occur during the white dwarf phase. Fig. 2 shows the evolution of a possible binary orbit and its first close approach during the white dwarf phase.

In [8] we show that the first close approach of a wide binary companion can lead to pollution even in Gyr old white dwarfs. The presence of a planet is not a necessity, although it can aid the scattering of planetesimals onto star-grazing orbits. The polluted white dwarf, WD 1009-184, with its companion at 6,870AU and an effective temperature of 9,940K (equivalent to a cooling age of $\sim$700Myr) [62, 89] stands out as an example system where this mechanism could be acting. Based on a wide binary fraction of $\sim$10%, we estimate that this mechanism could contribute to pollution in up to a few percent of any sample of white dwarfs. [89] present a sample of 17 white dwarfs with companions separated by more than 1,000AU, searched for Ca II with Keck/VLT and find that 5 are polluted, a similar rate to pollution in apparently single white dwarfs ($\sim$ 30% [87]).

3 Circumstellar material

Young stellar systems are characterised by the accretion of gas and dust onto the central star. Proto-planetary discs are the sites of complex gas and dust processes that potentially lead to grain growth and planet formation, as well as the clearing of the inner cavities during transition disc phases. The same stars, at the very end of their lives, when all that is left behind is a compact remnant, can again accrete material. The observations of gas and dust very close to some polluted white dwarfs tell us about these accretion processes in action. Whilst some similar physical processes

are shared by the accretion of material onto white dwarfs and in proto-planetary discs, the accretion rates and scales are very different. In many respects the circumstellar discs around polluted white dwarfs share more similarities with Saturn's rings.

3.1 Dust

Observations in the near-infrared of a sub-set of polluted white dwarfs find excess emission, over and above that predicted for the stellar photosphere. This emission is from dusty material at temperatures of around a thousand Kelvin. If such material is heated by the white dwarf, it will reside within a solar radius of the white dwarf, i.e. within the Roche limit. Asteroids that are scattered into this zone, will be disrupted by strong tidal forces. The observed dusty material is thought to originate in the disrupted bodies and accretes onto the white dwarf, leading to the observed pollution.

The first dusty white dwarf was observed in 1987, G29-38 [86], shortly after the discovery of the first debris disc around a main-sequence star [1], and before the first planets were discovered in 1991 [76]. Initially the debate in the literature regarded whether the emission was from a brown dwarf companion or dust [75, 65, 28, 26, 27, 64]. The infrared emission was linked to the presence of heavy elements discovered in the spectra by [39]. G29-38 remains one of the best studied dusty white dwarfs, with the largest infrared excesses, observed over wavelengths from K-band (2.2μm) to 24μm [59].

There are now over 40 dusty white dwarfs, all of which are polluted [20]. The frequency of infrared excess for white dwarfs has been characterised by several surveys, which reach a consensus of 1-5% [25, 17, 2, 13, 29, 47]. The majority of the white dwarfs where an infrared excess has been detected are warm stars, with $T_* > 10,000$K, with a few notable exceptions [81]. The rates of infrared excess are strikingly lower than the fraction of stars where pollution is detected of around 30%, e.g. [87, 88, 41].

Infrared spectroscopy of six dusty white dwarfs has revealed the presence of molecular emission features, most notably from silicates [31]. The dusty material accreting onto these polluted white dwarfs appears to have a composition similar to rocky material in our Solar System, and similar to the compositions derived from white dwarf pollution [82]. Future observations, for example using *MIRI* on *JWST*, will be well placed to further characterise the composition of the dust.

3.1.1 Structure of emitting dust

The observations constrain the temperature of the emitting dusty material; it clearly lies very close to the white dwarfs, generally within the tidal limit. The standard model, widely used in the literature to explain the observed emission is an opaque,

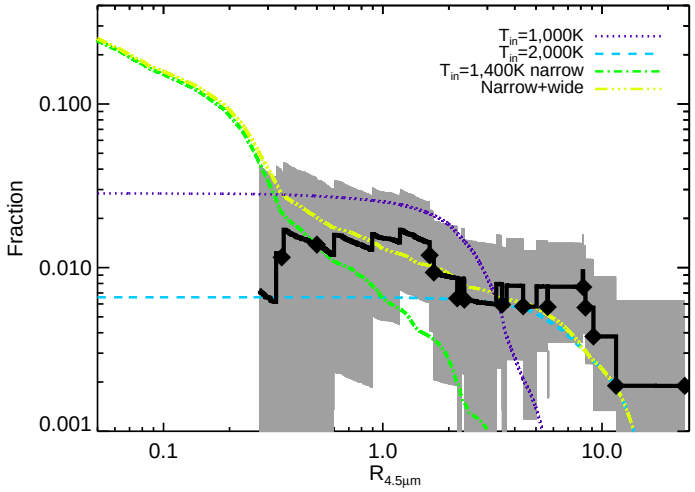

Fig. 3 Infrared observations of an unbiased sample of white dwarfs are consistent the presence of a wide, opaque, flat dust disc around up to 4%, whilst pollution occurs for around 30% of stars. Plotted is the cumulative distribution of infrared excesses (black); the number of stars in the sample with an infrared excess above a given level, divided by the number of stars for which such an excess is detectable, compared to four models in which all stars have a disc that extends from $T_{\rm in} = 1,000$K (purple) or $T_{\rm in} = 2,000$K to the Roche limit [9], or narrow discs from $T_{\rm in} = 1,400$K to $T_{\rm out} = 1,385$K.

flat dust disc, akin to Saturn's rings [30]. This dust disc must have a scale height that is significantly less than the white dwarf radius, in order that sufficient energy can be reprocessed by the disc to explain the observed infrared luminosities of the brightest objects [60]. The observed silicate emission features [31] must result from an optically thin region of the disc, such as a surface layer, or warped disc [32].

3.1.2 Accretion and dust

The dust observed close to white dwarfs supplies the accretion that is observed as pollution. A conundrum exists, however. The fraction of white dwarfs with an infrared excess (a few percent) is significantly lower than the fraction that are polluted (about 30%). [9] show that this discrepancy cannot be explained by opaque, flat dust discs that escape detection. At 4.5μm, observations with *Spitzer* or *WISE* should detect 95% of these discs, if they extend from $T_{in} = 1,200$K to the Roche limit.

In order to assess the frequency of dust around white dwarfs, [9] consider an unbiased sample of 528 white dwarfs with *Spitzer* and *WISE* observations collated from the literature. Fig. 3 plots the cumulative distribution of infrared excesses at 4.5μm (or W2) in this sample, this is the fraction of those white dwarfs where the observations are sensitive to a given excess, that have an infrared excess above the

given level. For comparison, the cumulative distribution of infrared excesses for a randomly selected 0.7% (4%) of the sample to have an opaque, flat dust disc with a temperature at the inner edge of $T_{\rm in} = 2,000$K (1,000K). This places an upper limit of 4% on the fraction of the sample that could have an opaque, flat dust disc that contains dust at temperatures hotter than 1,000K. The only way that all polluted white dwarfs could have an opaque dust disc is if those dust discs are narrow. The green line plots the cumulative distribution of infrared excesses assuming that 30% of the sample have an opaque, flat dust disc with a width of 15K (about 1% of the disc radius). Future observations that are sensitive to smaller infrared excesses would show a sharp increase in the fraction of white dwarfs with an infrared excess, if narrow dust discs are common.

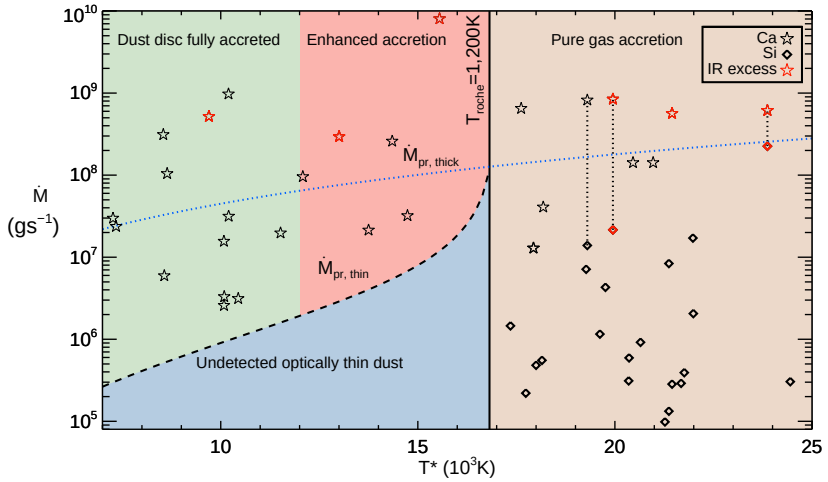

Fig. 4 The absence of an infrared excess for a polluted white dwarf can be explained by i) undetected optically thin dust (blue) 2) pure gas accretion, as dust sublimates directly (brown) 3) enhanced accretion of optically thin dust due to gas drag, or pure gas accretion (red) or 4) short dust disc lifetimes compared to sinking timescales (green). The dashed and dotted lines show the accretion rate due to Poynting-Robertson of undetected ($R_{4.5\mu m} = 0.3$) optically thin and optically thick dust disc, with an inner temperature of $T_{\rm in} = 1,200$K and $R_{\rm out} = R_{\rm roche}$. The accretion rates over plotted are from either Ca (stars) (Farihi, personal communication) or Si (diamonds) [41], assuming a composition of bulk Earth. Red symbols indicate the detection of an infrared excess.

Fig. 4 and [9] present four alternative explanations for the absence of an infrared excess, depending on the white dwarf's temperature and accretion rate. For the oldest white dwarfs, with the longest sinking timescales, the absence of an infrared excess can be explained by an opaque, flat dust disc that has been fully accreted, yet sustains detectable pollution (green region). The absence of an infrared excess for white dwarfs with low accretion rates ($< 10^7 {\rm gs}^{-1}$) can be sustained by the accretion, via Poynting-Robertson drag, of optically thin dust, whose infrared emission is below our detection limits, however, this dust must be replenished, if no variability

in the infrared excess or pollution is expected (blue region). For the hottest white dwarfs, dust that is released from a disrupting body and directly heated by the stellar radiation will sublimate. Those hot polluted white dwarfs without an infrared excess could have pure gas accretion, although the timescales for gas accretion are not well known (brown region). Warm white dwarfs with high accretion rates are the hardest to explain. It could be that the accreted material in these objects sublimates at lower temperatures ($\sim$ 900K), such that the brown region takes over the red region. Alternatively, the accretion of optically thin dust could be enhanced by the presence of gas. Future unbiased surveys that examine the occurrence of pollution, dust and gas in white dwarfs are key to understanding the full picture.

3.1.3 Variability

Recently, short term variability has been discovered around a dusty white dwarf WD J0959-0200 [84]. Within 300 days in 2010, its fluxes in 3.6 μm and 4.5 μm have decreased by $\sim$ 30% and the flux levels have remained unchanged ever since then. WD J0959-0200 also displays calcium triplet emission from an orbiting gas disc [18]. There are at least two scenarios that can explain the partial destruction of the dust disc. An impact of a small object onto a pre-existing dust disc or instability within the dust disc, possibly due to the coupling of the dust and gas [55, 45]. Further investigation is needed to understand the origin of the change of the infrared fluxes.

4 Compositions of the Accreting Planetesimals

Spectroscopic observations of polluted white dwarfs allow us to infer the chemical compositions of the accreting planetary material. There are about a thousand polluted white dwarfs know to-date and the majority were discovered in the Sloan Digital Sky Survey [15, 40]. Calcium is the most easily detected element in the optical wavelength range and it is the only element detected in most polluted white dwarfs. In order to measure the full composition, high resolution spectroscopic observations are required. There are only a handful of such objects that have been thoroughly studied [36]. In the optical range, we are mostly sensitive to the rock-forming elements, such as Ca, Mg, Si, Fe and O. The ultraviolet wavelength range is most ideal for detecting volatile elements, including C, S and N. So far, a total of 18 elements have been detected in a white dwarf's atmosphere, including C, O, Na, Mg, Al, Si, P, S, Ca, Sc, Ti, V, Cr, Mn, Fe, Ni, Zn and Sr. Here, we summarize the highlights of the compositions of extrasolar planetesimals and discuss the implications of these measurements.

4.1 Bulk Compositions

Our solar system is the best studied planetary system and can be used as a benchmark to understand other planetary systems. In terms of bulk composition, the best measurement comes from the analysis of meteorites, which are the building blocks of rocky planets. The standard picture is that planets formed by accreting from material in the surrounding area, which is strongly dependent on the temperature of the protoplanetary disc at a given location [42, 74]. The overall compositions of the solar system objects are a result of the temperature gradient of the protoplanetary disc: dry, rocky, terrestrial planets in the inner solar system and ice and gas giants in the outer solar system. CI chondrites are considered to be the most primitive object in the solar system and have a composition that closely resembles the solar composition [44]. Do extrasolar planetary systems have similar abundance patterns?

Fig. 5 shows the abundances of materials that have been accreted onto polluted white dwarfs [83]. The composition of bulk Earth and comet Halley are also shown for comparison. So far, the accreting material mostly resembles the composition of bulk Earth, which is dominated by four elements, O, Mg, Si and Fe. The only possible exception is #12 Ton 345, which has accreted a significant amount of carbon [37]. The relatively low oxygen abundance suggests the accreting material has little H_2O. The parent body is probably an analogue to dry Kuiper Belt Objects. However, the high carbon result is a bit controversial because a different group found a much lower carbon abundance by analysing the ultraviolet spectrum of Ton 345 [80].

In Fig. 5, #6 GD 61 and #11 WD J1242+5226 have accreted a significant amount of oxygen. Detailed abundance analysis shows that the oxygen is over abundant compared to the quantities required to combine with other observed elements to form typical rocky minerals, e.g. MgO, SiO_2, FeO or Fe_2O_3, CaO, Al_2O_3, etc. Therefore, the natural explanation for the oxygen over-abundance is that H_2O must be an important constituent of the accreting material [19, 54].

Note all white dwarfs shown in Fig. 5 sit in a "sweet spot" of 11,000 K to 23,000K. At a higher temperature, pollution could come from radiative levitation, which complicates the analysis [41]; at a lower temperature, dredge-up from the core could also bring material to the white dwarf's atmosphere [10]. No general trend is present in the abundance of the accreting material with respect to the white dwarf's effective temperature or the main sequence mass. It has been proposed that as the white dwarf cools/ages, the accreting material could change from asteroid-analog to comet-analog [6, 81]. High resolution spectroscopy for a large sample of white dwarfs at different temperatures is required to study the full range of compositions in exo-planetary asteroids.

4.2 Differentiation and Collisions

In the solar system, there are objects with very different compositions from the chondritic abundances. For example, iron meteorites are largely made from iron

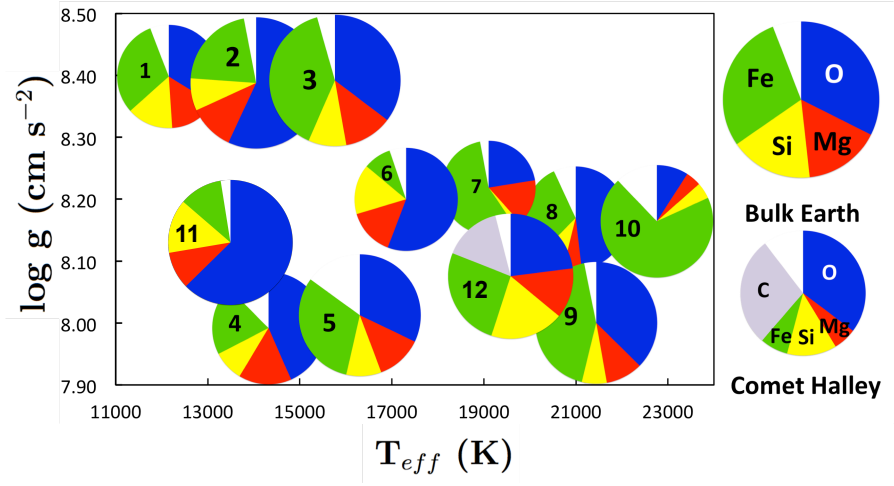

Fig. 5 A compilation of 12 white dwarfs with detections of at least O, Mg, Si and Fe (updated from [83]). The abscissa represents the effective temperature of the white dwarf, which is related its cooling age. The ordinate is surface gravity, which is connected to the main sequence mass. The mass fractions of the major elements are labelled. #12 Ton 345 is the only white dwarf that has accreted a planetesimal with a substantial amount of carbon. Here, the result from [37] is shown and please see section 4.1 for more details. Most white dwarfs have accreted extrasolar planetesimals with compositions similar to bulk Earth.

and probably come from the core of a differentiated parent body. The formation of Mercury is likely to involve the collision of two objects [3]. Differentiation and collisions can significantly change the compositions of extrasolar planetesimals; the formation of planets with non-chondritric compositions is inevitable [51].

One idea for exploring these effects is shown in Fig. 6, which looks for evidence for core and crust separation. Fe and Al are a representative core and crust element, respectively. The dispersion between Fe-to-Al ratios measured in polluted white dwarfs is much larger than the ratios measured in CI chondrites and planet-hosting stars. It shows that differentiation and collisions can be common in extrasolar planetary materials [34]. In addition, 16 heavy elements are detected in the parent body that is accreting onto the white dwarf GD 362. The best match solar system object with a similar composition is mesosiderite, a blend of core and crust material [82]. Evidence for differentiation and collision can be found in individual objects given enough elements are detected.

Plate tectonics can be closely related to a planet's habitability and its effect has been under intense investigation [66, 21]. Earth is the only known object that has undergone plate tectonics and an important outcome is the enrichment of the so called "incompatible" elements, e.g. Ba, Sr, in Earth's continental crust compared to other crust materials in the solar system. Polluted white dwarfs can be used to search for evidence of plate tectonics on extrasolar rocky objects. A pilot study on two objects were performed and upper limits of Ba-to-Ca ratios were obtained [35].

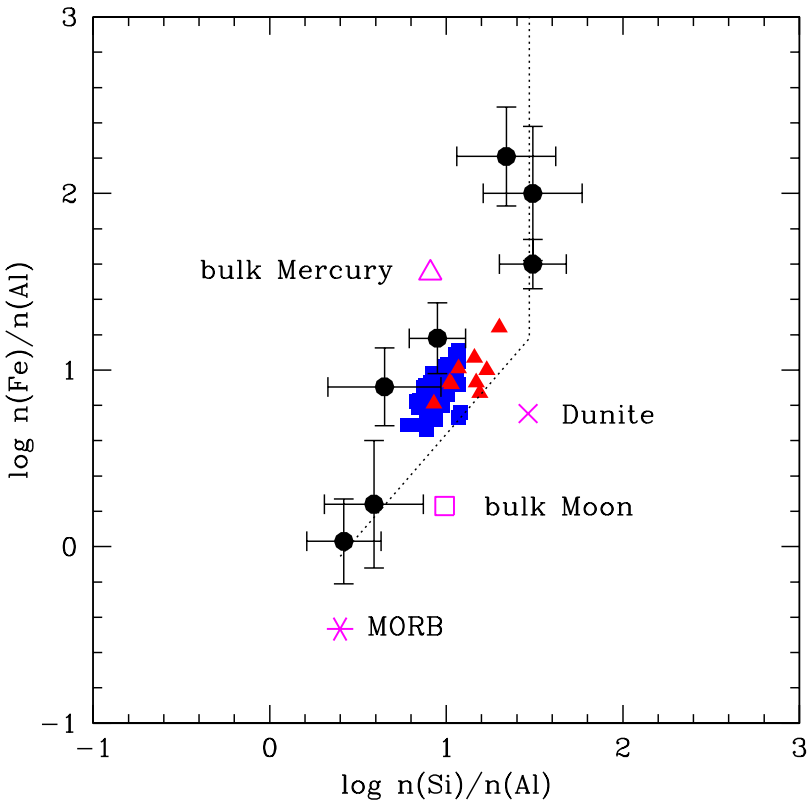

Fig. 6 Abundance ratios between Fe and Al versus Si and Al from materials accreted onto polluted white dwarfs (black dots), chondrites (red triangles) and planet-hosting stars (blue squares). A few solar system rocks are also included as magenta symbols [34]. Si and Al are typical crust material while Fe is mostly contained in the planetary core. The vertical black dotted line represents a model with a blend of core and mantle material while the sloped black dotted line represents a blend of core and crust material with 10% core by mass. The toy model can fit all the observed abundances in polluted white dwarfs. Chondrites and planet-hosting stars reside in a very small phase space. In addition, the dispersion between the Fe-to-Al ratios is much larger than that of Si-to-Al ratios, likely due to differentiation and collision.

No evidence for plate tectonics was found but this search should be extended to additional targets.

4.3 Implications

Planetesimals are the building blocks of planets and measuring their compositions can place strong constraint on planet formation models. For example, recent studies hypothesised that carbon planets could form around carbon-enhanced stars [4, 46]. So far, all the abundances observed in polluted white dwarfs have found low carbon abundances. Whatever the planet formation pathway it is, it must be universal in both the solar system and extrasolar planetary systems.

Tracing the volatile elements and locating the snow line/soot line is a key goal in the study of protoplanetary discs [43, 53]. One end result of volatiles are accreted onto the planetary objects in the system. Viewed as an ensemble, most white dwarfs are accreting from water-depleted extrasolar objects [33]. We are sampling drying rocky objects and this provides indirect evidence that snow lines can be present in other systems.

5 WD 1145+017: A White Dwarf with an Actively Disintegrating Asteroid

The tidal disruption of an asteroid is the standard model to explain white dwarf pollution [30]. However, the disintegrating asteroid has never been directly observed, until very recently.

5.1 Intriguing Light Curve

WD 1145+017 was observed in the first campaign of the extended *Kepler* mission. Multiple transits with periods around 4.5 hr were detected during the 80 day observation and significant evolutions were detected [67]. Ground-based follow-ups came quickly and the transit properties are very unique [11, 56, 23, 24]. (i) Transits are deep – transit depths as deep as 70% have been detected. (ii) Transit profiles are asymmetric – the egress lasts much longer than ingress. Similar transit profiles have been observed for disintegrating planets around main sequence stars. (iii) The transit duration is much longer than expected for a solid object. (iv) Light curve changes on a daily basis and it can be completely different after several weeks. A light curve is shown in Fig. 7.

The general consensus is that there is an actively disintegrating object around the white dwarf WD 1145+017. The transits are produced by dust coming off from the disintegrating objects. There are still many mysteries, particularly the long term evolution of the system [72]. How many fragments are there in the system? What is the dust production mechanism? What is the typical size and composition of the dust?

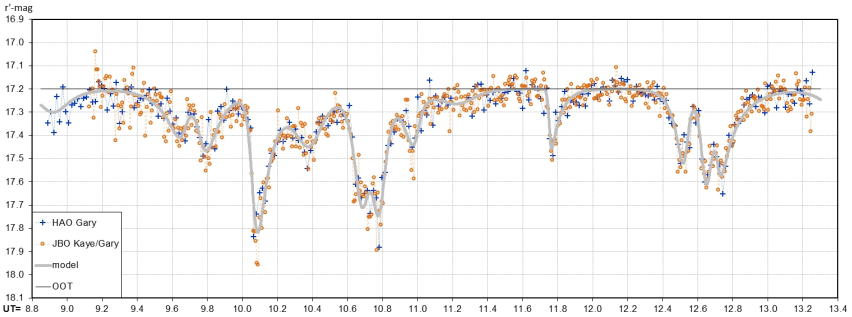

Fig. 7 A representative light curve of WD 1145+017 from the night of 2015 December 16, covering two full periods (updated from [56, 24]). The blue cross and yellow circle represents observations from the Gary 35 cm and Kaye 80cm telescope, respectively. The grey line is the model fit to the light curve and the black line is the out-of-transit level.

5.2 Infrared Excess

WD 1145+017 displays strong excess infrared radiation starting from the K band [67]. The SED can be fit by a warm disc within the tidal radius of the white dwarf, similar to the disc model discussed in section 3.1. However, it is puzzling that the dust disc is not aligned with the transiting objects [67, 85]. The infrared excess can also be fitted with a blackbody companion. Future observations, particularly near infrared spectroscopy, would reveal the nature of the infrared excess.

5.3 Polluted Atmosphere

High-resolution spectroscopic observations with the *Keck Telescope* of WD 1145+017 reveal 11 heavy elements, including O, Mg, Al, Si, Ca, Ti, V:, Cr, Mn, Fe and Ni, making it one of the most heavily polluted white dwarfs known [85]. The overall abundance pattern is very similar to those of CI chondrites, as shown in Figure 8. The relatively high oxygen abundance indicates the possibility of presence of water in the accreting material. However, further observations are required to confirm this due to the large uncertainty associated in the oxygen measurement [85]. High resolution ultraviolet spectroscopy would allow us to measure the abundances of volatile elements, such as C, S and possibly N so we could assess the volatile content of the accreting material.

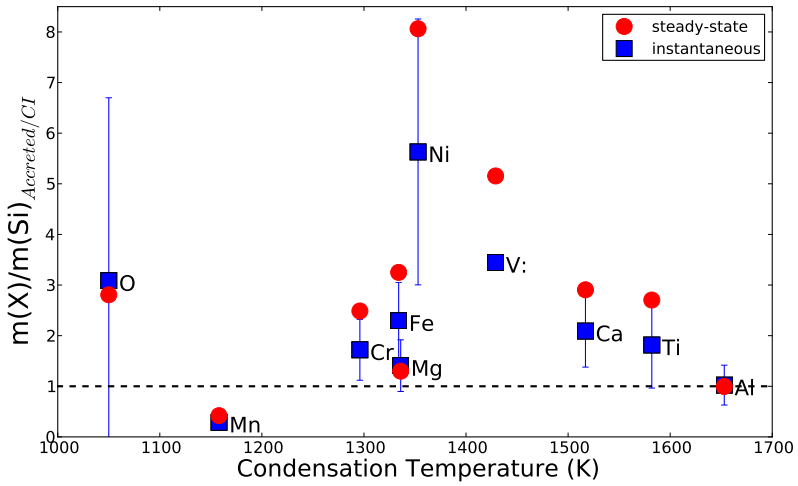

Fig. 8 Mass fraction of an element relative to Si in the material accreted onto WD 1145+017 and normalized to the ratios in CI chondrites [85]. Two models to derive the intrinsic abundances of the accreting material are presented, including the steady-state approximation and instantaneous model. Within the uncertainties, the overall abundance ratios are very similar to those observed in CI chondrites, consistent with abundances observed in other polluted white dwarfs (see Fig. 5).

5.4 Circumstellar Gas

High-resolution spectroscopic observations from *Keck* also discovered numerous absorption features from Mg, Ca, Ti, Cr, Mn, Fe and Ni around WD 1145+017. These features are broad, with a line width of ~ 300 km s^{-1}, asymmetric and deep, with an average depth about 15% below the continuum, as shown in Figure 9. They all come from transitions with a lower energy level between 0-3 eV [85]. These absorption lines are formed from circumstellar gas around WD 1145+017, likely associated with the disintegrating objects.

Previously, circumstellar gas has been detected around other white dwarfs, but none of them are morphologically similar to WD 1145+017. By monitoring the circumstellar features, [61] found that they change on a very short timescale. Further investigation is needed to understand the changes of the circumstellar feature.

6 Conclusions

In this chapter, we provide evidence that planetary systems around white dwarfs are common. Studying these systems can provide us with vital information regarding the formation and evolution of planetary systems, in particular the bulk compo-

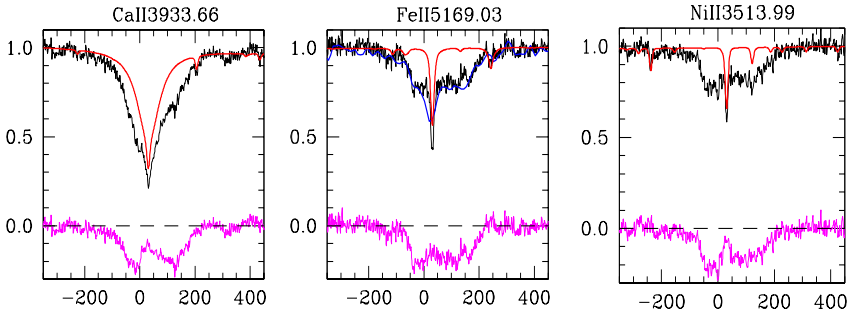

Fig. 9 Example of circumstellar feature detected around WD 1145+017 from [85]. The figure is shown in velocity space in the white dwarf's reference frame. The black and blue line represents data taken with Keck/HIRES and a slightly lower resolution spectrograph ESI a few weeks later. The red line represents the best model fit to the photospheric lines. The lower solid magenta line is the HIRES data minus the model – residual from circumstellar gas absorption.

sitions of extrasolar rocky objects. There is no other technique in the foreseeable future that will provide such good bulk compositions for rocky planetary material outside our Solar system. The recent discovery of an actively disintegrating asteroid around WD 1145+017 provides an exciting opportunity to study the real time tidal disruption processes and further our understanding of white dwarf planetary systems.

Acknowledgements We thank Bruce Gary and Saul Rappaport for updating Fig. 7 for this chapter.

References

1. Aumann, H.H., Beichman, C.A., Gillett et al., 1984, ApJL, 278, L23
2. Barber, S.D., Patterson, A.J., Kilic et al. 2012, ApJ, 760, 26
3. Benz, W., Slattery, W. L., & Cameron, A. G. W. 1988, ICARUS, 74, 516
4. Bond, J. C., O'Brien, D. P., & Lauretta, D. S. 2010, ApJ, 715, 1050
5. Bonsor, A., Wyatt, M. 2010, MNRAS, 409, 1631
6. Bonsor, A., Mustill, A. J., & Wyatt, M. C. 2011, MNRAS, 414, 930
7. Bonsor, A., Raymond, S.N., Augereau, 2013, MNRAS, 433, 2938
8. Bonsor, A., Veras, D., 2015, MNRAS, 454, 53
9. Bonsor, A., Farihi, J., Wyatt, M.. MNRAS, in prep (2016)
10. Brassard, P., Fontaine, G., Dufour, P., & Bergeron, P. 2007, 15th European Workshop on White Dwarfs, 372, 19
11. Croll, B., Dalba, P. A., Vanderburg, A., et al. 2015, arXiv:1510.06434
12. Debes, J.H., Sigurdsson, S. 2002, ApJ, 572, 556
13. Debes, J.H., Hoard, D.W., Kilic, M., et al., 2011, ApJ, 729, 4
14. Debes, J.H., Walsh, K.J., Stark, C., 2012, ApJ, 747, 148
15. Dufour, P., Bergeron, P., Liebert, J., et al. 2007, ApJ, 663, 1291
16. Duncan, M.J., Lissauer, J.J., 1998, Icarus, 134, 303
17. Farihi, J., Jura, M., Zuckerman, B., 2009, ApJ, 694, 805
18. Farihi, J., Gänsicke, B. T., Steele, P. R., et al. 2012, MNRAS, 421, 1635
19. Farihi, J., Gänsicke, B. T., & Koester, D. 2013, Science, 342, 218
20. Farihi, J.:, ArXiv e-prints (2016)
21. Foley, B. J., Bercovici, D., & Landuyt, W. 2012, Earth and Planetary Science Letters, 331, 281
22. Frewen, S.F.N., Hansen, B.M.S., 2014, MNRAS, 439, 2442
23. Gänsicke, B. T., Aungwerojwit, A., Marsh, T. R., et al. 2016, ApJL, 818, L7
24. Gary, B. L., Rappaport, S., Kaye, T. G., Alonso, R., & Hambsch, F.-J. 2016, arXiv:1608.00026
25. Girven, J., Brinkworth, C.S., Farihi, et al., 2012, ApJ, 749, 154
26. Graham, J.R., Matthews, K., Neugebauer, G., Soifer, B.T., 1990, ApJ, 357, 216
27. Graham, J.R., Reid, I.N., McCarthy, J.K., Rich, R.M., 1990, ApJL, 357, L21
28. Haas, M., Leinert, C., 1990, A&A, 230, 87
29. Hoard, D.W., Debes, J.H., Wachter, S., Leisawitz, D.T., Cohen, M., 2013, ApJ, 770, 21
30. Jura, M. 2003, ApJL, 584, L91
31. Jura, M., Farihi, J., Zuckerman, B., 2009, AJ, 137, 3191
32. Jura, M., Farihi, J., Zuckerman, B., Becklin, 2007, AJ, 133, 1927
33. Jura, M., & Xu, S. 2012, AJ, 143, 6
34. Jura, M., Xu, S., & Young, E. D. 2013, ApJL, 775, L41
35. Jura, M., Klein, B., Xu, S., & Young, E. D. 2014, ApJL, 791, L29
36. Jura, M., & Young, E. D. 2014, Annual Review of Earth and Planetary Sciences, 42, 45
37. Jura, M., Dufour, P., Xu, S., et al. 2015, ApJ, 799, 109
38. Kaib, N.A., Raymond, S.N., Duncan, M., 2013, Nature, 493, 381
39. Koester, D., Provencal, J., Shipman, H.L., 1997, A&A, 320, L57
40. Koester, D., Girven, J., Gänsicke, B. T., & Dufour, P. 2011, A&A, 530, A114
41. Koester, D., Gänsicke, B. T., & Farihi, J. 2014, A&A, 566, A34
42. Larimer, J. W. 1967, GCA, 31, 1215
43. Lecar, M., Podolak, M., Sasselov, D., & Chiang, E. 2006, ApJ, 640, 1115
44. Lodders, K. 2003, ApJ, 591, 1220
45. Metzger, B. D., Rafikov, R. R., & Bochkarev, K. V. 2012, MNRAS, 423, 505
46. Moriarty, J., Madhusudhan, N., & Fischer, D. 2014, ApJ, 787, 81
47. Mullally, F., Kilic, M., Reach, W.T., et al. 2007, ApJS, 171, 206
48. Murray, C.D., Dermott, S.F.: Solar system dynamics, 1999
49. Mustill, A.J., Villaver, E., 2012, ApJ, 761, 121
50. Mustill, A.J., Veras, D., Villaver, E. 2014, MNRAS, 437, 1404

51. O'Neill, H. S. C., & Palme, H. 2008, Philosophical Transactions of the Royal Society of London Series A, 366, 4205
52. Payne, M.J., Veras, D., Holman, M.J., Gänsicke, B.T., 2016, MNRAS, 457, 217
53. Qi, C., Öberg, K. I., Wilner, D. J., et al. 2013, Science, 341, 630
54. Raddi, R., Gänsicke, B. T., Koester, D., et al. 2015, MNRAS, 450, 2083
55. Rafikov, R. R., & Garmilla, J. A. 2012, ApJ, 760, 123
56. Rappaport, S., Gary, B. L., Kaye, T., et al. 2016, MNRAS, 458, 3904
57. Raymond, S.N., Armitage, P.J., Gorelick, N., 2010, ApJ, 711, 772
58. Raymond, S.N., Barnes, R., Veras, D., et al. 2009, ApJL, 696, L98
59. Reach, W.T., Kuchner, M.J., von Hippel, T., et al. 2005, ApJL, 635, L161
60. Reach, W.T., Lisse, C., von Hippel, T., Mullally, F., 2009, ApJ, 693, 697
61. Redfield, S., Farihi, J., Cauley, P. W., et al. 2016, arXiv:1608.00549
62. Sion, E.M., Holberg, J.B., Oswalt, T.D., McCook, G.P., Wasatonic, R., 2009, AJ, 138, 1681
63. Su, K.Y.L., Rieke, G.H., Stansberry, J.A., et al. 2006, ApJ, 653, 675
64. Telesco, C.M., Joy, M., Sisk, C., 1990, ApJL, 358, L17
65. Tokunaga, A.T., Hodapp, K.W., Becklin, E.E., et al., 1988, ApJL, 332, L71
66. Valencia, D., O'Connell, R. J., & Sasselov, D. D. 2007, ApJL, 670, L45
67. Vanderburg, A., Johnson, J. A., Rappaport, S., et al. 2015, Nature, 526, 546
68. Veras, D., Wyatt, M.C., Mustill, A.J., Bonsor, A., Eldridge, J.J., 2011, MNRAS, 417, 2104
69. Veras, D., Wyatt, M.C., 2012 MNRAS, 421, 2969
70. Veras, D., Mustill, A.J., Bonsor, A., Wyatt, M.C., 2013, MNRAS, 431, 1686
71. Veras, D., Mustill, A.J., Gänsicke, B.T., et al., 2016, MNRAS, 458, 3942
72. Veras, D., Marsh, T. R., Gnsicke, B. T. 2016, MNRAS
73. Villaver, E., Livio, M. 2007, ApJ, 661, 1192
74. Wetherill, G. W. 1990, Annual Review of Earth and Planetary Sciences, 18, 205
75. Wickramasinghe, N.C., Hoyle, F., Al-Mufti, S., 1988, APSS, 143, 193
76. Wolszczan, A., Frail, 1992, Nature, 355, 145
77. Wyatt, M.C., Smith, R., Su, K.Y.L., et al. 2007, ApJ, 663, 365
78. Wyatt, M.C, 2008, ARAA, 46, 339
79. Wyatt, M.C., Farihi, J., Pringle, J.E., Bonsor, A., 2014, MNRAS, 439, 3371
80. Wilson, D. J., Gänsicke, B. T., Koester, D., et al. 2015, MNRAS, 451, 3237
81. Xu, S., & Jura, M. 2012, ApJ, 745, 88
82. Xu, S., Jura, M., Klein, B., Koester, D., & Zuckerman, B. 2013, ApJ, 766, 132
83. Xu, S., Jura, M., Koester, D., Klein, B., & Zuckerman, B. 2014, ApJ, 783, 79
84. Xu, S., & Jura, M. 2014, ApJL, 792, L39
85. Xu, S., Jura, M., Dufour, P., & Zuckerman, B. 2016, ApJL, 816, L22
86. Zuckerman, B., Becklin, E.E. 1987, Nature, 330, 138
87. Zuckerman, B., Koester, D., Reid, I.N., Hünsch, M., 2003, ApJ, 596, 477
88. Zuckerman, B., Melis, C., Klein, B., Koester, D., Jura, M., 2010, ApJ, 722, 725
89. Zuckerman, B., 2014, ApJL, 791, L27